PNAS RESEARCH ARTICLE | EARTH, ATMOSPHERIC, AND PLANETARY SCIENCES

The triple oxygen isotope composition of marine sulfate and 130 million years of microbial control

Anna R. Waldeck[a,1,2], Jordon D. Hemingway[a,b], Weiqi Yao[a,c], Adina Paytan[d], and David T. Johnston[a]

Edited by Donald Canfield, Syddansk Universitet, Odense M., Denmark; received February 3, 2022; accepted June 13, 2022

The triple oxygen isotope composition ($\Delta'^{17}O$) of sulfate minerals is widely used to constrain ancient atmospheric pO_2/pCO_2 and rates of gross primary production. The utility of this tool is based on a model that sulfate oxygen carries an isotope fingerprint of tropospheric O_2 incorporated through oxidative weathering of reduced sulfur minerals, particularly pyrite. Work to date has targeted Proterozoic environments (2.5 billion to 0.542 billion years ago) where large isotope anomalies persist; younger timescale records, which would ground ancient environmental interpretation in what we know from modern Earth, are lacking. Here we present a high-resolution record of the $\delta^{18}O$ and $\Delta'^{17}O$ in marine sulfate for the last 130 million years of Earth history. This record carries a $\Delta'^{17}O$ close to 0‰, suggesting that the marine sulfate reservoir is under strict control by biogeochemical cycling (namely, microbial sulfate reduction), as these reactions follow mass-dependent fractionation. We identify no discernible contribution from atmospheric oxygen on this timescale. We interpret a steady fractional contribution of microbial sulfur cycling (terrestrial and marine) over the last 100 million years, even as global weathering rates are thought to vary considerably.

barite | marine sulfate | triple oxygen isotopes | Cenozoic | Cretaceous

Significance

Stable isotopes in marine sulfate preserve information about Earth's climate. Interpretations of geologic marine sulfate records infer changes in weathering states, microbial activity, volcanic events, and even atmospheric oxygen levels in Earth's deep past. Here we construct a record of the minor ^{17}O isotope in marine sulfate over the last 130 million years. In interpreting this new isotope record, we determine that the changes are consistent with a microbially dominated sulfur cycle over the last 100+ million years. Further, the ^{17}O isotope composition of marine sulfate does not preserve a signal of atmospheric O_2 over this interval.

The global biogeochemical sulfur cycle is tightly linked to that of carbon, oxygen, and iron, which, together, govern Earth's climate and redox budget over time (1, 2). Specifically, weathering of reduced sulfur minerals (e.g., pyrite, FeS_2) consumes atmospheric oxygen (O_2) and generates a net release of carbon dioxide (CO_2) on geologic timescales (3, 4). Meanwhile, pyrite burial results in a net flux of O_2 to the atmosphere and drawdown of CO_2 over those same timescales. A memory of this recycling is captured in the stable isotope composition of seawater sulfate (5), which, since 130 million years ago (Ma), is most faithfully recorded by marine barite ($BaSO_4$) minerals (6–10). The sulfur isotope record ($\delta^{34}S$) of marine barite (9–11) has classically been interpreted as reflecting a balance of terrestrial weathering (3, 12), microbial reworking (13), and sedimentary export from the ocean (10, 14, 15), with recent suggestions of an outsized control via sulfur injected through LIP emplacement (16). In parallel, the marine barite oxygen isotope record ($\delta^{18}O$) is thought to largely reflect changes in microbial recycling, here linking gross metabolism to environmental features like the locus of organic matter oxidation, sea level, and nutrient availability (7, 15).

In addition to the biogeochemical information contained in "major" isotope records ($\delta^{34}S$, $\delta^{18}O$), recent work highlights the potential for the "minor" oxygen isotope composition of sulfate (here reported as $\Delta'^{17}O$; *Materials and Methods*) to track atmospheric pO_2/pCO_2 and gross primary productivity (GPP) in the geologic past (17, 18). This minor isotope proxy is based on the presumption that between 10% and 25% of O atoms in sulfate produced from pyrite weathering originate from atmospheric O_2 (19, 20). Tropospheric O_2 contains a large, negative ^{17}O anomaly ($\Delta'^{17}O < 0$) that is a balance of stratospheric exchange reactions, where pO_2/pCO_2 sets the absolute magnitude of the effect (21), and dilution by gross primary production at Earth's surface (GPP) (22). If oxidative weathering transfers O atoms from O_2 to sulfate, then, by extension, the $\Delta'^{17}O$ of sulfate can be used to first estimate the $\Delta'^{17}O$ composition of ancient atmospheric O_2, which, in turn, is related to pO_2/pCO_2 and GPP. However, these interpretations require that 1) significant amounts of O_2 are directly incorporated into sulfate and 2) such signals are not subsequently overprinted by biogeochemical cycling. Further, it is well documented that pyrite oxidation can and does proceed in anoxic environments (e.g., with Fe^{3+}), with the suggestion that the resultant sulfate $\delta^{18}O$ is only tied to H_2O oxygen (23, 24). Recent $\Delta'^{17}O$ work on modern river systems dominated by pyrite weathering (25), a high-precision characterization of modern seawater sulfate (5), and a 6-million-year-old seawater sulfate mineral archive (26) challenge both these requirements, leaving the exact nature of the information captured by this proxy in question.

Author affiliations: [a]Department of Earth and Planetary Sciences, Harvard University, Cambridge, MA 02138; [b]Geological Institute, Department of Earth Sciences, ETH Zürich, 8092 Zürich, Switzerland; [c]Department of Ocean Science and Engineering, Southern University of Science and Technology, 518055 Shenzhen, China; and [d]Institute of Marine Science, University of California, Santa Cruz, CA 95064

Author contributions: A.R.W., A.P., and D.T.J. designed research; A.R.W. performed research; A.P. contributed new reagents/analytic tools; A.R.W., J.D.H., W.Y., A.P., and D.T.J. analyzed data; and A.R.W., J.D.H., W.Y., A.P., and D.T.J. wrote the paper.

The authors declare no competing interest.

This article is a PNAS Direct Submission.

[1]To whom correspondence may be addressed. Email: annawaldeck@northwestern.edu.

[2]Present address: Department of Earth and Planetary Sciences, Northwestern University, Evanston, IL 60208

This article contains supporting information online at https://www.pnas.org/lookup/suppl/doi:10.1073/pnas.2202018119/-/DCSupplemental.

Published July 26, 2022.

As a means of bridging between the intellectual framework that has guided the reconstruction of Precambrian environments and that which is captured by the modern ocean, rivers, and recent past, here we report a high temporal resolution triple oxygen isotope record of marine barite ($BaSO_4$) minerals from 14 globally distributed sediment cores. Marine barite is precipitated in the open ocean water column during organic matter remineralization (27) and has been shown to faithfully capture the isotope composition of marine sulfate (10, 15, 26). By interpreting $\Delta'^{17}O$ alongside $\delta^{18}O$ and $\delta^{34}S$, together with independent estimates of critical environmental variables such as the pyrite weathering flux, marine sulfate reservoir size, and sulfate inputs from volcanism, we provide a complete biogeochemical context for interpreting the triple oxygen isotope composition of marine sulfate across the last 130 million years.

Results

The oxygen isotope composition ($\delta^{18}O$ and $\Delta'^{17}O$) of seawater sulfate is inferred from measurements of marine barite minerals sampled from seafloor sediments collected from 14 globally distributed sites (*SI Appendix*, Table S1). Samples were screened for alteration based on scanning electron microscopy, X-ray diffraction (XRD), previously published Sr and S isotope data, and consistency with background temporal trends (see *SI Appendix*, Text for a full discussion). This screening affects the statistical treatment (i.e., regression CIs) but has no significant effect on the global interpretations. After filtering, samples of similar age yield statistically indistinguishable estimates for marine sulfate oxygen isotope composition; here we use a 1σ uncertainty interval based on the directly measured variability within modern core-top barite (± 0.5‰ for $\delta^{18}O$ and ± 0.020‰ for $\Delta'^{17}O$) (15, 26) as a conservative estimate. Oxygen isotope measurements from this study are compiled along with previous records of $\delta^{34}S$ (Fig. 1*A*) (9–11, 15). We apply a previously calibrated offset between barite and seawater sulfate for $\delta^{18}O$ of -2.7‰ (15, 26), whereas the $\delta^{34}S$ and $\Delta'^{17}O$ directly record seawater sulfate composition (10, 26).

The $\delta^{18}O$ and $\Delta'^{17}O$ of seawater sulfate both vary over the last 130 million years. In the Cretaceous (older than 65 million years), marine sulfate $\delta^{18}O$ ranges from 11 to 18‰ and is noticeably more variable than younger records (Fig. 1*B* and *C*). Over the Cenozoic (65 million years to present), the $\delta^{18}O$ of marine sulfate decreases steadily from 14 to 8.7‰. The $\Delta'^{17}O$ composition of marine sulfate (Fig. 1*C*) varies noticeably relative to a 1σ analytical uncertainty of 0.020‰. Here, compositions range between -0.042‰ and $+0.063$‰, with an overall positive trend toward the present (slope $= 0.0003$; $R^2 = 0.23$; p-val < 0.0001). Across our whole dataset, $\Delta'^{17}O$ correlates negatively with $\delta^{18}O$ (slope $= -0.005$; $R^2 = 0.24$; p-val < 0.0001). Over the last 40 million years, marine sulfate $\delta^{18}O$ correlates positively with $\delta^{34}S$ (slope $= 3.07$; $R^2 = 0.63$; p-val < 0.0001). Between 40 million and 90 million years, $\delta^{18}O$ does not significantly correlate with $\delta^{34}S$ (slope $= -0.19$; $R^2 = 0.114$; p-val < 0.007). We tested the covariance of marine sulfate $\delta^{18}O$ and $\delta^{34}S$ through time (details in *SI Appendix*, Text and Fig. S5).

Discussion

The most striking feature of this >100-million-year time series is the apparent lack of an atmospheric O_2 signal. Although consistent with observations in the modern and recent past, this opens the question of just how sulfate comes to adopt an oxygen isotope composition through time. Further, the mechanisms often

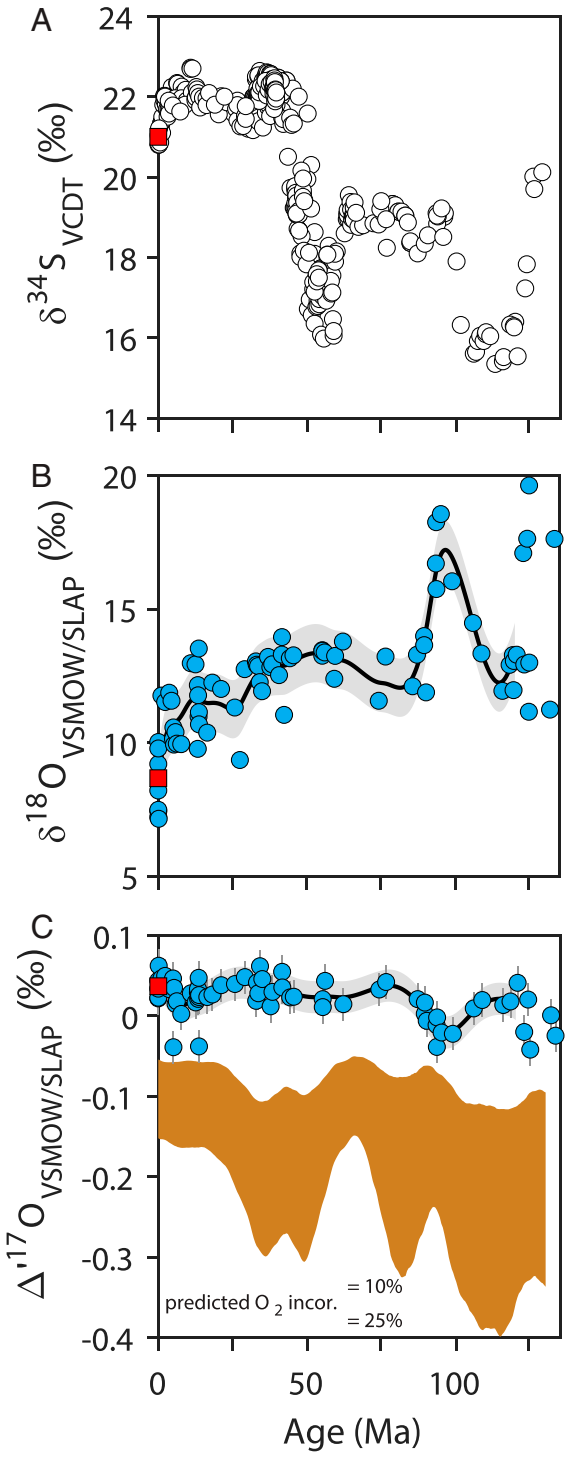

Fig. 1. Marine sulfate (*A*) $\delta^{34}S$ (9, 10, 12, 15, 28), (*B*) $\delta^{18}O$ (this study), and (*C*) $\Delta'^{17}O$ (this study) (*y* axes) are plotted versus age in millions of years (*x* axes). The standard reference frames are Vienna-Canyon Diablo Triolite (VCDT) and Vienna-Standard Mean Ocean Water/Standard Light Antarctica Precipitation (VSMOW/SLAP) for sulfur and oxygen isotopes, respectively. Modern marine sulfate in each panel is represented by the red square (5, 29, 30). Error bars denote the analytical precision associated with the long-term reproducibility of standards ($1\sigma = 0.2$‰ for $\delta^{34}S$, $1\sigma = 0.3$‰ for $\delta^{18}O$, and $1\sigma = 0.020$‰ for $\Delta'^{17}O$). Note that the $\delta^{18}O$ of marine barite is corrected here for the -2.7‰ offset from seawater sulfate. A bootstrapped, smoothing spline regression of the $\delta^{18}O$ and $\Delta'^{17}O$ time series is included. The gray line is the averaged spline fit, and the gray shaded region reflects the 2σ CI based on modern core-top barite (± 0.5‰ for $\delta^{18}O$ and ± 0.020‰ for $\Delta'^{17}O$) (15, 26). The shaded brown curve in *C* reflects the prediction for marine sulfate $\Delta'^{17}O$ if it incorporates between 10% and 25% of oxygen from atmospheric O_2. This calculation follows the method of ref. 31, with varied pCO_2 according to predictions by ref. 32 and constant pO_2 and GPP.

discussed as the drivers of the $\delta^{18}O$ in sulfate—weathering, microbial activity (specifically, microbial sulfate reduction [MSR]) and volcanism—all carry consequences for the companion $\delta^{34}S$. Thus, there is also a simple requirement of internal consistency. In what follows, we consider all these features and work toward a better understanding of both what is controlling the barite record and how it could be different from on early Earth.

(De)Coupling S and O. Isotope studies of sulfate in modern rivers, marine sediment pore waters, and microbial experiments demonstrate that sulfate $\delta^{34}S$ and $\delta^{18}O$ are often positively correlated. In a global compilation of river sulfate isotope measurements (*SI Appendix*, Fig. S8 and Dataset S2, $n = 919$), this relationship, in part, arises from the relative contributions of cold, pyrite-rich, high weathering-rate catchments (often characterized by lower-$\delta^{18}O$ waters) that have low sulfate $\delta^{34}S$ and $\delta^{18}O$. This is then balanced by warm, wet catchments with thick soil mantles (where waters are likely to be more enriched in $\delta^{18}O$) that have high sulfate $\delta^{34}S$ and $\delta^{18}O$. River biogeochemistry also overprints the initial weathered sulfate signal, with ties to the meteoric water line. A similar positive relationship is observed in numerous pore water environments dominated by MSR and in experiments targeting this metabolism (6, 33). In these latter cases, the rates of MSR govern the (non)linearity of the relationship. Important in all cases is that the rate of isotopic change in S and O can vary (34).

Similarly, the marine barite record presented here captures periods of positive correlation between $\delta^{34}S$ and $\delta^{18}O$ (the expectation) but also intervals with high degrees of $\delta^{34}S$ change and little to no $\delta^{18}O$ change (Fig. 2). For the last 40 million years, the slope of change in marine sulfate $\delta^{18}O$ vs. $\delta^{34}S$ is ~3, which is between the observed slope of change in global rivers (~0.6) and in sulfate that is influenced by slow rates of MSR (≫3). Prior to 40 million years ago, however, the dramatic oscillations in $\delta^{34}S$ (~6‰) are accompanied by only modest changes in $\delta^{18}O$ (~1‰). This could result from differing seawater sulfate concentrations (35), or in the actual drivers of the sulfur cycle itself. For example, recent work on the Cenozoic–Cretaceous $\delta^{34}S$ record of marine barite forwarded the hypothesis that volcanic sulfur, sourced via the emplacement of large igneous provinces (LIPs), may be responsible for the rapid changes in the $\delta^{34}S$ record (16). As outgassed S oxidation would differ between subareal and submarine volcanism, an opportunity may exist to decouple sulfur and oxygen isotopes. Further, the $\Delta'^{17}O$ composition of sulfate may provide additional information about this hypothesis. For example, in the case of the ~35 Ma subareal Afro-Arabian igneous province, volcanic SO_2 is expected to incorporate a positive $\Delta'^{17}O$ anomaly during atmospheric oxidation to sulfuric acid (36). Conversely, submarine oxidation would be water buffered and carry no such large anomaly. Across the entire marine barite record, we do not observe the expected pulses of $\Delta'^{17}O > 0$ as one might predict from the $\delta^{34}S$ derived LIP hypothesis (16). This could result from several scenarios. The $\delta^{34}S$ LIP hypothesis could be incorrect or overestimate volcanic sulfur fluxes, or a primary LIP-derived $\Delta'^{17}O$ was overprinted via microbial activity, bringing the observed oxygen isotope composition back toward an equilibrium with water. This latter suggestion would allow LIPs to influence the $\delta^{34}S$ but not be preserved in the oxygen isotope records.

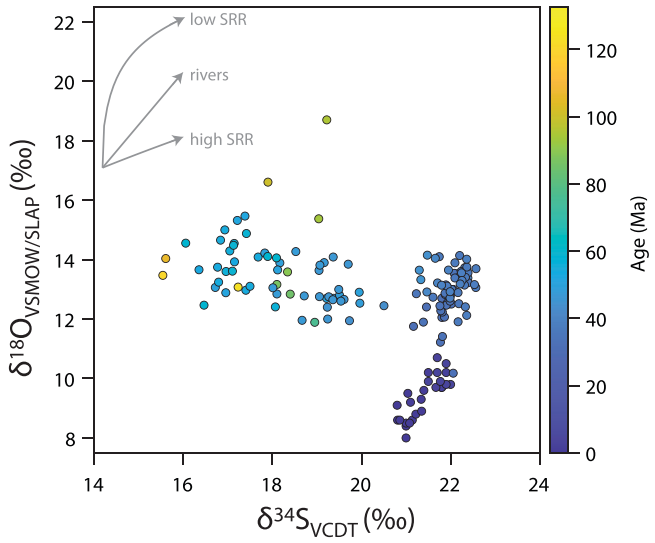

Fig. 2. The marine sulfate stable isotope record ($\delta^{34}S$, *x* axis, versus $\delta^{18}O$, *y* axis). Marker face colors reflect the age of each sample (see colorbar). Each filled circle reflects an individual sample with both $\delta^{18}O$ and $\delta^{34}S$ data. Vectors in the upper left-hand corner reflect the direction of isotope change associated with the river sulfate flux and with MSR (high sulfate reduction rate and low sulfate reduction rate).

Interpretive Framework for the $\Delta'^{17}O$ of Sulfate. Traditionally, the $\Delta'^{17}O$ in marine sulfate is attributed to contributions related to local water and the partial incorporation of atmospheric O_2 (modern O_2 $\Delta'^{17}O = -0.501 \pm 0.011$‰ (37). With water assumed to be near zero in $\Delta'^{17}O$, all (negative) nonzero $\Delta'^{17}O$ compositions are interpreted to come directly from O_2 (18). The variance in an observed $\Delta'^{17}O$ signal is then, at the geologic formation level, interpreted as differing fractional degrees of O_2 incorporation or water buffering via MSR (33, 38). On longer geological timescales, variability is attributed to changes in the influence of GPP on atmospheric composition. In parallel to simple two-component mixing between O_2 and water, kinetic and equilibrium isotope effects like those catalyzed via MSR can influence sulfate oxygen isotope composition (38). These isotope effects are mass dependent, meaning they lead to much smaller $\Delta'^{17}O$ effects than that generated in atmospheric O_2. As quantifications of kinetic effects in this system are lacking, we use, instead, theoretical predictions of equilibrium isotope effects to approximate the influence of microbial sulfur cycling (38, 39). Here we find the inclusion of mass-dependent fractionation crucial to the interpretation of the smaller-magnitude $\Delta'^{17}O$ changes in marine sulfate from the Cretaceous to Cenozoic.

In the context of the global biogeochemical sulfur cycle, the primary source of sulfate to the ocean is via terrestrial weathering of pyrite (FeS_2) and evaporite dissolution ($CaSO_4$) (40). Pyrite oxidation is traditionally thought to directly incorporate atmospheric O_2 (knowing also that anoxic oxidation via Fe^{3+} is common), while evaporite dissolution reintroduces ancient seawater with a sulfate oxygen isotope composition reflective of its depositional age. In turn, previous studies have emphasized differing controls on the isotopic composition of riverine sulfate. The relative proportion of sulfate derived from weathered pyrite [estimated global average $\delta^{34}S = -17$‰ and $\delta^{18}O = +2$‰ (41)] to that of weathered evaporite [estimated global average $\delta^{34}S = +16$‰ and $\delta^{18}O = +12$‰ (41)] is a main factor thought to set the combined river sulfate isotope composition (23, 42, 43). More recent work demonstrates that the near-full range of $\delta^{34}S$ and $\delta^{18}O$ is also possible from weathering a single, fixed lithology, here emphasizing the role of MSR in addition to host rock in setting the composition of riverine sulfate (25). In general, MSR occurs in anoxic waters where sulfate serves as the electron acceptor during oxidation of organic matter. Reduced hydrogen sulfide can be sequestered as pyrite (FeS_2) where iron is available, or it can be reoxidized to sulfate, with a new oxygen isotope composition dependent on that of environmental water

(33, 44) and the environmental oxidant. As discussed above, there is a characteristic isotope effect associated with MSR, where residual sulfate develops an enrichment in both $\delta^{34}S$ and $\delta^{18}O$. In marine sediment pore waters where MSR is the dominant process influencing the isotope composition of sulfate, the residual sulfate pool can reach compositions of $\delta^{34}S$ between +20‰ and +70‰ and $\delta^{18}O$ from +22‰ to +26‰ higher than pore fluid H_2O (34). The maximum observed $\delta^{18}O$ in pore water sulfate most commonly approaches the predicted equilibrium isotope offset from water (45). Enrichments in riverine sulfate are similar, but here sulfate $\delta^{18}O$ is tied to a variable meteoric water $\delta^{18}O$. In both settings, the simplest interpretation is that, albeit microbially catalyzed, the oxygen isotope composition of sulfate approaches that of equilibrium between sulfate and local water.

The $\Delta'^{17}O$ of sulfate can be used to test and extend the hypotheses noted above. For example, in the case where MSR is setting the oxygen isotope composition of sulfate, the $\delta^{17}O$ and $\delta^{18}O$ composition should evolve along a fixed slope reflective of a given mass law, noted as θ (defined as the slope of $\ln(\delta^{17}O/1{,}000 + 1)$ vs. $\ln(\delta^{18}O/1{,}000 + 1)$). This manifests as a straight line with a modestly negative slope in Fig. 3*B*, again where the magnitude of the imparted $\Delta'^{17}O$ is a function of $\delta^{18}O$. Similar triple oxygen isotope relationships would result from various water–sulfoxy anion equilibrium effects. These could carry slight differences in θ (see ref. 39). Conversely, if the composition of sulfate does, indeed, carry a memory of atmospheric O_2 incorporation, it is possible to deviate from these relationships. In the pyrite weathering–dominated Marsyangdi River system (25), the isotopic composition of sulfate covers a wide span ($\delta^{18}O$ = −12.6‰ to +11.4‰ and $\Delta'^{17}O$ = +0.041‰ to +0.180‰) and is defined by a slope of $\theta = 0.526 \pm 0.002$. In the Mississippi River (47), sulfate oxygen isotope compositions evolve along a statistically indistinguishable slope from that of the Marsyangdi, $\theta = 0.524 \pm 0.008$.* It is then internally consistent that modern seawater sulfate [$\delta^{18}O = 8.7 \pm 0.3$‰ and $\Delta'^{17}O = 0.037 \pm 0.016$‰ (5)], interpreted as, in part, reflective of riverine inputs, lies statistically within the array defined by Marsyangdi River sulfate (Fig. 3). This framework naturally then extends to the entire Cenozoic–Cretaceous marine sulfate record, which again falls along this same trajectory (with a statistically indistinguishable $\theta = 0.525 \pm 0.003$; Fig. 3). The commonality across modern river sulfate, modern seawater sulfate, and the Cretaceous to Cenozoic marine barite record suggests a shared set of controls.

If microbial metabolism (MSR and otherwise) catalyzes an isotopic equilibrium with water as predicted by $\delta^{18}O$ studies (33), then theoretical equilibrium fractionation predictions can help refine a mechanistic understanding of the observed isotopic relationships. Quantum mechanical modeling, specifically, density functional theory, allows for calculations of specific triple oxygen isotope offsets tethered to local waters (meteoric or seawater itself) (39). The most parsimonious explanation of the Cretaceous–Cenozoic record is then contributions from both riverine sulfate and an MSR-catalyzed equilibrium with seawater. This is presented in Fig. 3*B* by the area bound by dashed lines and buttressed by the isotope equilibrium predictions of SO_4^{2-} (dark gray field) and SO_3–OH^- (light gray field). As expected, equilibrium with a seawater-like composition would fall along the right edge of this field. This result supports previous interpretations of the $\delta^{34}S$ and $\delta^{18}O$ records as reflecting a mixture of riverine contributions and marine recycling, a sulfur cycle under microbial control (48).

Linking the Sulfur Cycle and Long-Term Weathering. As noted above, perhaps the most striking feature of the data is the empirical consistency between the oxygen isotope compositions ($\Delta'^{17}O$ vs. $\delta^{18}O$) of riverine sulfate, modern seawater sulfate, and the record of the marine sulfate reservoir over the last 130 million years as they all relate to a microbially catalyzed equilibrium with water. The variability within the barite record can then be most simply interpreted as a balance of two contributions: that which is adopted from rivers (J_{riv}) and the degree to which MSR in marine sediments further resets the composition of sulfate (J_{bio}). This framework was initially used to describe the modern sulfate budget (5), but herein is applied to the entire Cenozoic–Cretaceous record (see *SI Appendix*, Text for full details). We do

*The larger variability in the Mississippi slope is a function of less overall $\delta^{18}O$ variability ($\delta^{18}O$ = −3.6 to 8.8‰). The $\Delta'^{17}O$ is also slightly offset, as discussed in ref. 38. Finally, we note that the Mississippi may reflect additional mechanisms (i.e., contributions from anthropogenic sources).

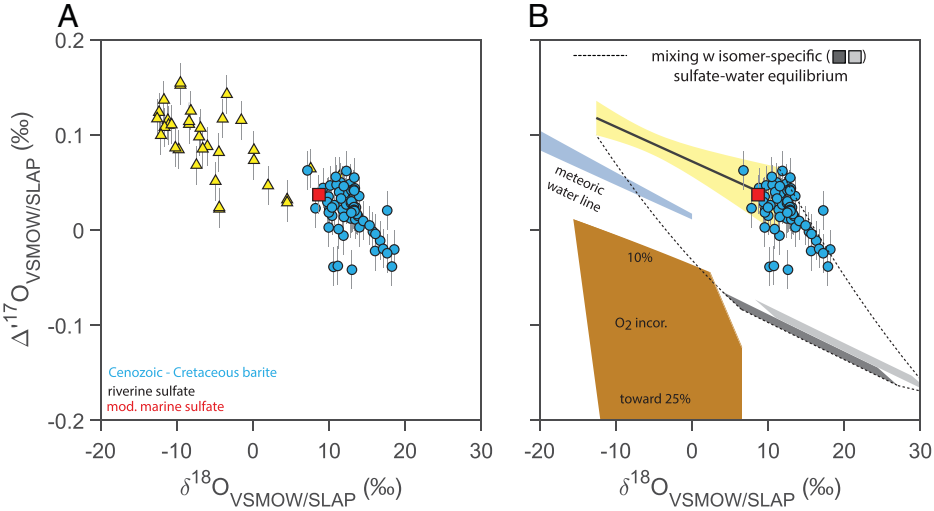

Fig. 3. (*A*) The triple oxygen isotope ($\Delta'^{17}O$ and $\delta^{18}O$) composition of Marsyangdi River sulfate (yellow triangles) (25) and Cenozoic–Cretaceous seawater sulfate (blue circles, this study) and the mean value of modern seawater sulfate (red square, $n = 24$) (5). (*B*) Here, the Cenozoic–Cretaceous seawater sulfate data are placed against an array for modern meteoric water (in blue) (46) and predictions for sulfate that carry both an equilibrium component (dashed field) and atmospheric O_2 component (between 10% and 25%, brown field). The yellow field reflects a best fit and CI for riverine sulfate (25). For equilibrium, we use two different isomers of sulfate tied to the entire meteoric water line, noting that seawater anchors the enriched end of this array.

so noting that this extension is imperfect, and fluxes outside of that included here could be contributing at lower levels, but try to note these uncertainties in turn.

The first question to address is the constancy of the equilibrium endmember and riverine sulfate over time; only after this can temporal changes in the sulfur cycle be meaningfully extracted and interpreted. For marine recycling and MSR, the isotopic composition of seawater H_2O and/or environmental temperature may influence the oxygen isotope composition of J_{bio}. We do not consider any change in $\delta^{18}O_{H_2O}$ of seawater, but do vary temperatures between 4 °C and 15 °C, consistent with predictions for the last 100 million years (49–51). Further, the controls on isotopic equilibrium offset would also remain unchanged, together meaning that the "MSR equilibrium" end-member should remain relatively uniform. In the case of rivers, it is certainly plausible that the globally integrated isotopic composition of riverine sulfate varies over time and as a function of features like exhumed lithologies, contributions from terrestrial/riverine MSR, and the isotope composition of environmental water with which sulfate equilibrates. Although impossible to measure in the past, we propose that the heterogeneity of modern river systems serves as a useful proxy for the sort of changes one might see over time. To account for variation in $\delta^{18}O$ of J_{riv}, we use the full interquartile range (25th to 75th percentiles) of a global riverine sulfate dataset (Dataset S2), or 1.3 to 10.4‰. Detailed riverine $\Delta'^{17}O$ sulfate data are, indeed, more limited, with uncertainty surrounding the source of positive $\Delta'^{17}O$ anomaly in headwater sulfates and the exact θ for MSR. As such, we move forward only using $\delta^{18}O$ arguments, but note that the inclusion of $\Delta'^{17}O$ should be revisited as more constraints arise.

We pair this two-component mixing model with a prediction for global weathering rate over the last 100 million years (52) to probe the relationship between riverine and microbial contributions. First, the flux of riverine sulfate input to the oceans is scaled to the total sedimentary weathering flux over the last 100 million years, following ref. 3, to solve for J_{riv}. From our mixing, with error propagated, J_{bio} can be directly constrained. Notably, this leaves riverine contributions dominating the oxygen isotope composition of marine sulfate over much of this period, with J_{bio} estimates between 0 and $1.2{\cdot}10^{12}$ mol/y (Fig. 4). It is only in the mid-Cretaceous, where riverine fluxes are predicted to decrease to roughly 10% of present value, that biology exerts a more prominent control. This is consistent with an enriched $\delta^{18}O$ and a depleted $\Delta'^{17}O$ at that time, indicating more MSR-equilibrated sulfate, perhaps related to the expansion of the Cretaceous interior seaway. Across much of the Cenozoic, the riverine sulfate flux is modeled as increasing by eightfold, while J_{bio} is roughly constant. These results suggest that the global rate of marine sedimentary MSR is decoupled from riverine sulfate inputs to the ocean. Ultimately, the combined effects of pyrite weathering and riverine biogeochemistry (specifically, MSR) come to largely set the isotopic composition of seawater sulfate.

All of these interpretations carry significance for previous story lines for the sulfate record. A consequence of the Cenozoic–Cretaceous barite record is that it stands in contrast with the canonical interpretation of direct O_2 incorporation used for Precambrian pO_2/pCO_2 and GPP estimates. Recall that the pyrite weathering–dominated Marsyangdi River contributes sulfate with $\Delta'^{17}O > 0$‰, the opposite in sign than would be expected if O_2 were involved (25). The evolution of this signal downstream, the result of biogeochemistry (i.e., both recycling within MSR and HS^- oxidation), falls along an array that is indistinguishable from equilibrium with water. Similarly, the Cenozoic–Cretaceous record of marine barite holds no (yet) resolvable fraction of atmospheric oxygen (the brown field in Fig. 3*B*). The question at hand then becomes what changed between the Proterozoic and more modern sulfur cycles. Further study is needed of the processes and environments that give rise to atmospheric O_2 incorporation into sulfate.

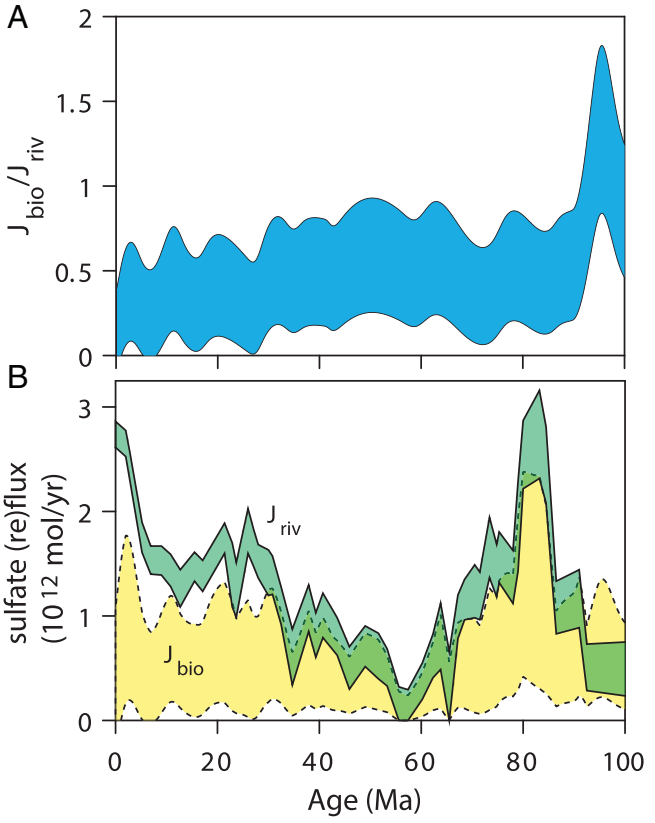

Fig. 4. (*A*) Predictions for J_{bio}/J_{riv} over the last 100 million years are calculated from the two-component mixing model and marine sulfate $\delta^{18}O$ record. (*B*) Sedimentary weathering rate (52) is used to constrain J_{riv} (3). The flux magnitude of J_{bio} is estimated using the predictions in *A*.

Conclusions

The triple oxygen isotope composition of marine sulfate mineral records is a powerful tool for paleoenvironmental reconstructions. Here, we employed high-fidelity marine barite records from sediment cores to inform the evolution of the sulfur cycle over the last 130 million years. The data reveal a different sulfur cycle from that captured in the Precambrian, but strikingly consistent with that observed in modern rivers and seawater sulfate as well as previous work on the S cycle (9). Here, the triple oxygen isotope composition of sulfate is governed by an evolving balance between biogeochemical recycling and weathering, with continental weathering playing an outsized role. To this end, it is also clear that atmospheric oxygen does not significantly influence the oxygen isotope composition of sulfate. However, our result pointing to the importance of rivers, and noting that terrestrial ecosystems have changed dramatically over Earth history, poses an interesting and testable hypothesis about the capacity to impart a mass-independent effect in marine seawater sulfate.

Materials and Methods

The materials and methods are detailed here; further information is provided in *SI Appendix*. All data used in this study are reported in Datasets S1 and S2.

Sample Collection and Chemical Methods. Marine barite samples were collected from 14 Integrated Ocean Drilling Program and Deep Sea Drilling Project sites, and seven core-top locations, across the global ocean. Barite was first extracted from sediments following a sequential dissolution method (15, 53) and further cleaned by dissolution in sodium carbonate (15, 54, 55). In the sequential dissolution method, samples were immersed in a series of solutions in order to remove various nonbarite minerals. In sequence, the sediments sat in HCl to dissolve carbonates, sodium hypochlorite to oxidize organic matter, hydroxylamine hydrochloride to remove iron and manganese oxyhydroxides, concentrated HF–HNO_3 mixtures with ratios of 1:2, 1:1, and 2:1 to remove silicates, and aluminum chloride in 1M HNO_3 to remove fluorides. After each dissolution step, the samples were rinsed and centrifuged three times in deionized (DI) water. Finally, the remaining barite was collected onto filter paper and heated at 750 °C in the furnace for 1 h to oxidize highly refractory organic matter. Following these steps, samples were weighed and added to Teflon (polytetrafluoroethylene) vials with a 0.5 M Na_2CO_3 solution in a ratio of 10 mg of $BaSO_4$ to 2 mL of Na_2CO_3 solution. The sample mixtures were sonicated at room temperature for 60 min and then placed in an 80 °C oven for 16 h. The sodium carbonate step was performed three times. After the third collection, barium chloride was added (10% $BaCl_2$ in 2M HCl) until samples reached pH < 2, to precipitate $BaSO_4$. Samples were rinsed two times in 2N HCl and three times in DI water, and dried at 60 °C.

Isotope Notation. We use standard isotope notation throughout this work. The amount of a minor isotope (^{34}S, ^{18}O) relative to a major isotope (^{32}S, ^{16}O), is expressed as

$$\delta^{x}Y = \left(\frac{{}^{x}R_{sample}}{{}^{x}R_{standard}} - 1 \right) \cdot 1{,}000‰, \quad [1]$$

where ${}^{x}R$ is the ratio of minor to major isotope in a sample or standard material. Standards are Vienna-Canyon Diablo Triolite (V-CDT) for sulfur and Vienna Standard Mean Ocean Water/Standard Light Antarctica Precipitation (VSMOW/SLAP) for oxygen. The triple oxygen isotope composition of sulfate describes the ratio $^{17}O/^{16}O$ relative to $^{18}O/^{16}O$. This relationship is expressed in the form

$$\Delta'^{17}O = \left[\ln\left(\frac{\delta^{17}O}{1{,}000} + 1 \right) - \theta_{RL} \cdot \ln\left(\frac{\delta^{18}O}{1{,}000} + 1 \right) \right] \cdot 1{,}000‰. \quad [2]$$

We use $\theta_{RL} = 0.5305$, which is also the theoretical high-temperature limit for the linear dependence of $^{17}O/^{16}O$ versus $^{18}O/^{16}O$ (56). All measurements are expressed in units of permil.

Isotope Measurements. Purified barite was then subjected to two different forms of isotope analyses. First, $\sim 250 \pm 50$ μg of clean dry barite was weighed in triplicate into silver capsules (Elemental Micoranalysis; 4×3.2 mm) with AgCl and glassy C additive in an $\sim$2:1 mass ratio. Before measurement, weighed sample capsules were dried at 60 °C in a vacuum oven overnight. All samples were run using a high-temperature conversion elemental analyzer (TC/EA) connected to a Thermo Scientific Delta V Plus isotope ratio mass spectrometer configured in a continuous flow mode. The $\delta^{18}O$ data were corrected to accepted values for for standards International Atomic Energy Agency (IAEA)-SO-5 and National Bureau of Standards (NBS)-127 and NBS-127 (57). Samples were corrected for 1) the amount of additive, which contributes $<$10% to the area of the CO peak; 2) drift over the course of the analysis; and 3) scale compression. All isotope ratios are reported in units of permil relative to VSMOW/SLAP. The long-term weighted 1σ for the standards is $<0.6‰$ ($n = 282$).

For minor oxygen isotope analyses, barite was measured according to published protocols (58). Approximately 5 mg of purified $BaSO_4$ was reacted in a pure F_2 atmosphere by heating with a 50-W CO_2 laser, which liberates O_2 along with other fluorinated byproducts. Sample gas was passed through multiple cryofocus steps and an in-line gas chromatograph before being introduced, as pure O_2, to a Thermo Scientific MAT 253 gas source isotope ratio mass spectrometer configured in dual-inlet mode. Each $\delta^{18}O$ and $\delta^{17}O$ were taken as the mean of four acquisitions of 10 cycles with a target of 3,000 mV to 5,000 mV on the m/z 34 cup. The measured $\delta^{17}O$ and $\delta^{18}O$ values were subsequently corrected for the fractionation associated with lasing and gas purification (58). This correction uses the fraction of original SO_4 collected as O_2, the $\delta^{18}O$ and $\delta^{17}O$ from the 253 analysis, and the true $\delta^{18}O$ sample value from TC/EA analysis. Using a set of internal standards, we report a precision on sulfate of 0.02‰ for $\Delta'^{17}O$ ($n = 76$). Information on tank gas calibration and potential Ar interference are provides in *SI Appendix*, as well as details on the applied three-point calibration (air O_2, University of Wisconsin Garnet-2, NBS 28).

Data Availability. All study data are included in the article and/or supporting information.

ACKNOWLEDGMENTS. We thank Julien Foriel for laboratory assistance, members of the D.T.J. group for helpful discussions, Nir Galili for XRD analyses, and two anonymous reviewers for feedback that improved the manuscript. This research was supported by NSF Grant OCE-1821958 (D.T.J. and A.R.W.), NSF Grant OCE-1946137 (D.T.J. and A.R.W.), NSF Grant OCE-1946153 (A.P.), and NSF Grant OCE-1821976 (A.P.).

1. J. M. Hayes, J. R. Waldbauer, The carbon cycle and associated redox processes through time. *Philos. Trans. R. Soc. Lond. B Biol. Sci.* **361**, 931–950 (2006).
2. D. A. Fike, A. S. Bradley, C. V. Rose, Rethinking the ancient sulfur cycle. *Annu. Rev. Earth Planet. Sci.* **43**, 593–622 (2015).
3. M. A. Torres, A. J. West, G. Li, Sulphide oxidation and carbonate dissolution as a source of CO_2 over geological timescales. *Nature* **507**, 346–349 (2014).
4. E. K. Berner, R. A. Berner, *Global Environment: Water, Air, and Geochemical Cycles* (Princeton University Press, 2012).
5. A. Waldeck *et al.*, Deciphering the atmospheric signal in marine sulfate oxygen isotope composition. *Earth Planet. Sci. Lett.* **522**, 12–19 (2019).
6. A. V. Turchyn, D. P. Schrag, R. Coccioni, A. Montanari, Stable isotope analysis of the Cretaceous sulfur cycle. *Earth Planet. Sci. Lett.* **285**, 115–123 (2009).
7. A. V. Turchyn, D. P. Schrag, Cenozoic evolution of the sulfur cycle: Insight from oxygen isotopes in marine sulfate. *Earth Planet. Sci. Lett.* **241**, 763–779 (2006).
8. A. V. Turchyn, D. P. Schrag, Oxygen isotope constraints on the sulfur cycle over the past 10 million years. *Science* **303**, 2004–2007 (2004).
9. A. Paytan, M. Kastner, D. Campbell, M. H. Thiemens, Seawater sulfur isotope fluctuations in the Cretaceous. *Science* **304**, 1663–1665 (2004).
10. A. Paytan, M. Kastner, D. Campbell, M. H. Thiemens, Sulfur isotopic composition of cenozoic seawater sulfate. *Science* **282**, 1459–1462 (1998).
11. W. Yao *et al.*, A revised seawater sulfate S-isotope curve for the Eocene. *Chem. Geol.* **532**, 119382 (2020).
12. W. Yao, S. Markovic, A. Paytan, A. M. Erhardt, U. G. Wortmann, Quantifying pyrite oxidation on continental shelves during the onset of Antarctic glaciation in the Eocene-Oligocene transition. *Earth Planet. Sci. Lett.* **568**, 117015 (2021).
13. B. B. Jørgensen, Mineralization of organic matter in the sea bed–The role of sulphate reduction. *Nature* **296**, 643–645 (1982).
14. U. G. Wortmann, A. Paytan, Rapid variability of seawater chemistry over the past 130 million years. *Science* **337**, 334–336 (2012).
15. S. Markovic, A. Paytan, H. Li, U. G. Wortmann, A revised seawater sulfate oxygen isotope record for the last 4 Myr. *Geochim. Cosmochim. Acta* **175**, 239–251 (2016).
16. T. A. Laakso, A. Waldeck, F. A. Macdonald, D. Johnston, Volcanic controls on seawater sulfate over the past 120 million years. *Proc. Natl. Acad. Sci. U.S.A.* **117**, 21118–21124 (2020).
17. H. Bao, J. R. Lyons, C. Zhou, Triple oxygen isotope evidence for elevated CO_2 levels after a Neoproterozoic glaciation. *Nature* **453**, 504–506 (2008).
18. P. W. Crockford *et al.*, Claypool continued: Extending the isotopic record of sedimentary sulfate. *Chem. Geol.* **513**, 200–225 (2019).
19. N. Balci, W. C. Shanks III, B. Mayer, K. W. Mandernack, Oxygen and sulfur isotope systematics of sulfate produced by bacterial and abiotic oxidation of pyrite. *Geochim. Cosmochim. Acta* **71**, 3796–3811 (2007).
20. I. Kohl, H. Bao, Triple-oxygen-isotope determination of molecular oxygen incorporation in sulfate produced during abiotic pyrite oxidation (pH=2–11). *Geochim. Cosmochim. Acta* **75**, 1785–1798 (2011).
21. M. H. Thiemens, History and applications of mass-independent isotope effects. *Annu. Rev. Earth Planet. Sci.* **34**, 217–262 (2006).
22. B. A. Killingsworth *et al.*, Towards a holistic sulfate-water-O_2 triple oxygen isotope systematics. *Chem. Geol.* **588**, 120678 (2022).
23. K. E. Relph *et al.*, Partitioning riverine sulfate sources using oxygen and sulfur isotopes: Implications for carbon budgets of large rivers. *Earth Planet. Sci. Lett.* **567**, 116957 (2021).
24. D. Calmels, J. Gaillardet, A. Brenot, C. France-Lanord, Sustained sulfide oxidation by physical erosion processes in the Mackenzie River basin: Climatic perspectives. *Geology* **35**, 1003–1006 (2007).
25. J. D. Hemingway *et al.*, Triple oxygen isotope insight into terrestrial pyrite oxidation. *Proc. Natl. Acad. Sci. U.S.A.* **117**, 7650–7657 (2020).
26. A. R. Waldeck *et al.*, Calibrating the triple oxygen isotope composition of evaporite minerals as a proxy for marine sulfate. *Earth Planet. Sci. Lett.* **578**, 117320 (2022).
27. A. Paytan, S. Mearon, K. Cobb, M. Kastner, Origin of marine barite deposits: Sr and S isotope characterization. *Geology* **30**, 747–750 (2002).
28. W. Yao, A. Paytan, Possible triggers of the seawater sulfate S-isotope increase between 55 and 40 million years ago. *Chem. Geol.* **552**, 119788 (2020).
29. C. Rees, W. Jenkins, J. Monster, The sulphur isotope geochemistry of ocean water sulphate. *Geochim. Cosmochim. Acta* **42**, 377–382 (1978).
30. D. T. Johnston *et al.*, Placing an upper limit on cryptic marine sulphur cycling. *Nature* **513**, 530–533 (2014).
31. X. Cao, H. Bao, Dynamic model constraints on oxygen-17 depletion in atmospheric O_2 after a snowball Earth. *Proc. Natl. Acad. Sci. U.S.A.* **110**, 14546–14550 (2013).

32. G. L. Foster, D. L. Royer, D. J. Lunt, Future climate forcing potentially without precedent in the last 420 million years. *Nat. Commun.* **8**, 14845 (2017).
33. E. Bertran *et al.*, Oxygen isotope effects during microbial sulfate reduction: Applications to sediment cell abundances. *ISME J.* **14**, 1508–1519 (2020).
34. G. Antler, A. V. Turchyn, V. Rennie, B. Herut, O. Sivan, Coupled sulfur and oxygen isotope insight into bacterial sulfate reduction in the natural environment. *Geochim. Cosmochim. Acta* **118**, 98–117 (2013).
35. T. K. Lowenstein, L. A. Hardie, M. N. Timofeeff, R. V. Demicco, Secular variation in seawater chemistry and the origin of calcium chloride basinal brines. *Geology* **31**, 857–860 (2003).
36. E. Martin, I. Bindeman, Mass-independent isotopic signatures of volcanic sulfate from three supereruption ash deposits in Lake Tecopa, California. *Earth Planet. Sci. Lett.* **282**, 102–114 (2009).
37. J. A. Wostbrock, E. J. Cano, Z. D. Sharp, An internally consistent triple oxygen isotope calibration of standards for silicates, carbonates and air relative to VSMOW2 and SLAP2. *Chem. Geol.* **533**, 119432 (2020).
38. X. Cao, H. Bao, Small triple oxygen isotope variations in sulfate: Mechanisms and applications. *Rev. Mineral. Geochem.* **86**, 463–488 (2021).
39. J. Hemingway, M. L. Goldberg, K. M. Sutherland, D. T. Johnston, *Theoretical estimates of sulfoxyanion triple-oxygen equilibrium isotope effects and their implications. ESSOAr* [Preprint] (2022). https://doi.org/10.1002/essoar.10508624.1. Accessed 15 April 2022.
40. I. Halevy, S. E. Peters, W. W. Fischer, Sulfate burial constraints on the Phanerozoic sulfur cycle. *Science* **337**, 331–334 (2012).
41. G. E. Claypool, W. T. Holser, I. R. Kaplan, H. Sakai, I. Zak, The age curves of sulfur and oxygen isotopes in marine sulfate and their mutual interpretation. *Chem. Geol.* **28**, 199–260 (1980).
42. E. I. Burt *et al.*, Conservative transport of dissolved sulfate across the Rio Madre de Dios floodplain in Peru. *Geology* **49**, 1064–1068 (2021).
43. A. Burke *et al.*, Sulfur isotopes in rivers: Insights into global weathering budgets, pyrite oxidation, and the modern sulfur cycle. *Earth Planet. Sci. Lett.* **496**, 168–177 (2018).
44. B. Brunner *et al.*, The reversibility of dissimilatory sulphate reduction and the cell-internal multi-step reduction of sulphite to sulphide: Insights from the oxygen isotope composition of sulphate. *Isotopes Environ. Health Stud.* **48**, 33–54 (2012).
45. R. E. Zeebe, A new value for the stable oxygen isotope fractionation between dissolved sulfate ion and water. *Geochim. Cosmochim. Acta* **74**, 818–828 (2010).
46. Z. Sharp, J. Wostbrock, A. Pack, Mass-dependent triple oxygen isotope variations in terrestrial materials. *Geochem. Perspect. Lett.* **7**, 27–31 (2018).
47. B. A. Killingsworth, H. Bao, I. E. Kohl, Assessing pyrite-derived sulfate in the Mississippi River with four years of sulfur and triple-oxygen isotope data. *Environ. Sci. Technol.* **52**, 6126–6136 (2018).
48. D. E. Canfield, The evolution of the earth surface sulfur reservoir. *Am. J. Sci.* **304**, 839–861 (2004).
49. N. Galili *et al.*, The geologic history of seawater oxygen isotopes from marine iron oxides. *Science* **365**, 469–473 (2019).
50. K. Wallmann, The geological water cycle and the evolution of marine $\delta^{18}O$ values. *Geochim. Cosmochim. Acta* **65**, 2469–2485 (2001).
51. J. Veizer *et al.*, Oxygen isotope evolution of phanerozoic seawater. *Palaeogeogr. Palaeoclimatol. Palaeoecol.* **132**, 159–172 (1997).
52. G. Li, H. Elderfield, Evolution of carbon cycle over the past 100 million years. *Geochim. Cosmochim. Acta* **103**, 11–25 (2013).
53. A. Paytan, M. Kastner, F. P. Chavez, Glacial to interglacial fluctuations in productivity in the equatorial Pacific as indicated by marine barite. *Science* **274**, 1355–1357 (1996).
54. G. N. Breit, E. Simmons, M. Goldhaber, Dissolution of barite for the analysis of strontium isotopes and other chemical and isotopic variations using aqueous sodium carbonate. *Chem. Geol. Isot. Geosci. Sect.* **52**, 333–336 (1985).
55. K. Von Allmen, M. E. Böttcher, E. Samankassou, T. F. Nägler, Barium isotope fractionation in the global barium cycle: First evidence from barium minerals and precipitation experiments. *Chem. Geol.* **277**, 70–77 (2010).
56. X. Cao, Y. Liu, Equilibrium mass-dependent fractionation relationships for triple oxygen isotopes. *Geochim. Cosmochim. Acta* **75**, 7435–7445 (2011).
57. W. A. Brand *et al.*, Comprehensive inter-laboratory calibration of reference materials for $\delta^{18}O$ versus VSMOW using various on-line high-temperature conversion techniques. *Rapid Commun. Mass Spectrom.* **23**, 999–1019 (2009).
58. B. R. Cowie, D. T. Johnston, High-precision measurement and standard calibration of triple oxygen isotopic compositions ($\delta^{18}O$, $\delta^{17}O$) of sulfate by F_2 laser fluorination. *Chem. Geol.* **440**, 50–59 (2016).

PNAS
www.pnas.org

Supplementary Information for

Cenozoic and Cretaceous marine sulfate triple oxygen isotope record

Anna R. Waldeck, Jordon D. Hemingway, Weiqi Yao, Adina Paytan, and David T. Johnston

Anna R. Waldeck.
E-mail: annawaldeck@northwestern.edu

This PDF file includes:

Other supplementary materials for this manuscript include the following:

Supporting Information Text

Data Handling.

Scale calibration. The first aspect of data analysis that we consider is the calibration of our tank gas and the establishment of our VSMOW/SLAP scale. As presented in Figure S1, we correct our reference gas to the VSMOW/SLAP scale using most recently accepted values for silicate standards and air O_2 (1). From here, we apply a 3 point calibration (UWG-2, NBS 28 and air O_2). As such, given the inclusion of mass-independent O_2, calibration also takes into account scale compression issues on the larger $\Delta'^{17}O$ values that sulfate may carry. This calibration then includes materials that are fluorinated (silicates), as sulfates would be, as well as O_2, which by-passes the need for fluorination and is directly injected into the GC that sits before the mass spectrometer. Finally, it has been suggested that Argon can interfere with the measurement of especially atmospheric O_2. As seen in Figure S1, we run both Ar-bearing and Ar-free gas samples and they are statistically identical. As such, we can quantitatively rule out Ar contamination as a problem.

Wet chemistry. The barite extraction and reprecipitation methods employed here are well-rooted in the barite stable isotope literature (2–6) and have been specifically tested and used for sulfate oxygen isotopes as well (7). For example, to test the reliability of sulfate oxygen isotopes of barite in residues following the sequential leaching extraction from sediments, mixtures of ≈90% barite and ≈10% contaminating phases were prepared and processed (7). Further, to check that sodium carbonate reprocessing methods do not affect the sulfate oxygen isotopes of barite of sediment extraction residues, a mixture of ≈99% barite and ≈1% quartz and goethite were used (7). These methods have proven reliable for obtaining sulfate oxygen isotopes of barite for sample residues obtained from sediment samples that have high barite content and have not undergone significant diagenetic alteration.

Isotopic outliers. We observe a fraction of the barite data population with $\delta^{18}O$ values that fall below the overall marine barite $\delta^{18}O$ record (by 3 to 15‰) (Figure S2, left panel, red empty symbols). Here we define 'outliers' as those samples that have $\delta^{18}O$ values that are outside of the 3σ confidence interval determined by the $\delta^{18}O$ measurements of coretop barite (n=7). Recall that the seawater sulfate reservoir is well mixed and thus barite at any given time should be precipitating from an isotopically homogeneous reservoir (8). Through this vetting, a total of 13 outliers were identified. Due lower sample density and a higher degree of variance in the $\delta^{18}O$ record between 115 and 135 million years ago, we are unable to distinguish outliers in this time interval. Most outliers are from site 577 within the age interval of 50-65 Ma, with a few samples from other sites (two samples from site 766A, one sample each from a coretop and sites 574C, 865B, and 551). We envision three possible reasons for deviation in sample $\delta^{18}O$ from the general trend: (1) the barite crystals underwent some degree of diagenetic alteration *in situ*, (2) the samples contained pyrite minerals that were oxidized during sample processing, or (3) the barite samples which are separated from sediments using a sequential leaching procedure (9) contained other mineral phases which contributed to the signal. Below we outline our further reasoning and analyses that we applied to the samples to assess the causes for the observed deviations.

1) Our collective data do not support diagenetic alteration as the main factor contributing to samples with low $\delta^{18}O$ values in our dataset. *In situ* diagenetic alteration of barite minerals can lead to characteristic barite morphologies (10) and deviations in Sr and/or S isotope compositions of the barite. SEM analyses of samples with 'outlier' $\delta^{18}O$ values did not reveal diagenetically derived barite. Likewise, the outlier samples were not distinguishable based on available literature constraints for $^{87}Sr/^{86}Sr$ and $\delta^{34}S$ (2, 4, 11, 12).

2) We do not find that oxidation of pyrite during sample processing is a concern for the samples with low $\delta^{18}O$ values. Pyrite oxidation during extraction of barites from sediment samples (which involves leaching the sediments with acidic solutions) can be a source of concern for samples with significant weight % pyrite (13, 14). This is not consistent with porewater and sediment records for these sites which are sulfate rich and do not contain measurable pyrite. Moreover, based on the scale of the $\delta^{18}O$ offset (in many cases 5-10‰), formation of sulfate via oxidation of sulfide would not be feasible because of isotope mass balance constraints. Pyrite oxidation would contribute sulfate with roughly $\delta^{18}O$=0‰ (based on a lab water $\delta^{18}O$=-5‰), and thus to account for the measured $\delta^{18}O$ of the outliers, close to 100% of the barite would originate from pyrite oxidation.

3) We do note that in cases where the sediment sample residue contained low levels of barite relative to other mineral phases, it is possible that oxygen from other, non-barite minerals contributed to the observed signal. Imaging of the samples with a scanning electron microscope (SEM) showed that the majority of outliers contained low levels of barite <50% and high levels of other contaminating phases (Figure S3) in samples post-sediment extraction and pre-secondary processing via Na_2CO_3 method. Our applied extraction methods are thoroughly tested (see above), however these tests may not be relevant to samples that contain <50% barite after extraction from sediments.

Subsequent X-ray diffraction (XRD) analyses of a subset of Na_2CO_3-processed "outlier" samples and those with expected $\delta^{18}O$ revealed that all samples are pure barite. XRD patterns were obtained on a Empyrean (PANalytical) diffractometer using a Cu-ka (1.54184Å) X-ray source and a Lynxeye detector. Patterns were obtained by step scanning from 5° to 50° 2 in 0.01° increments at a scan rate of 0.40° per minute. The X-ray diffractograms were automatically compared with the International Center for Diffraction Data (ICDD) database.

In sum, the internal consistency and data density over the entire record suggests that it is recording a primary signal. The exact source of the 'outliers' remains unclear, however given the criteria from above, these data are excluded from ensuing analyses/interpretations.

Table S1. List of core locations and metadata for each core.

Hole		Location
1207B	IODP	37°47.433'N 162°45.053'E
1218A	IODP	8°53.378'N, 135°22.00'W
1219A	IODP	7°48.019'N, 142°00.940'W
1221C	IODP	12°01.999'N, 143°41.572'W
1333C	IODP	10°30.996'N, 138°25.159'W
1337C	IODP	3°50.009'N, 123°12.352'W
574A	DSDP	4°12.52'N, 133°19.81'W
574C	DSDP	4°12.52'N, 133°19.81'W
766A	DSDP	19°54'S, 110°30'E
849D	IODP	0°10.993'N, 110°31.167'W
851B	IODP	2°46.223'N, 110°34.308'W
305	DSDP	32°00.13'N, 157°51.00'E
551	DSDP	48°54.64'N, 13°30.09'W
577	DSDP	32°26.51'N, 157°43.40'E

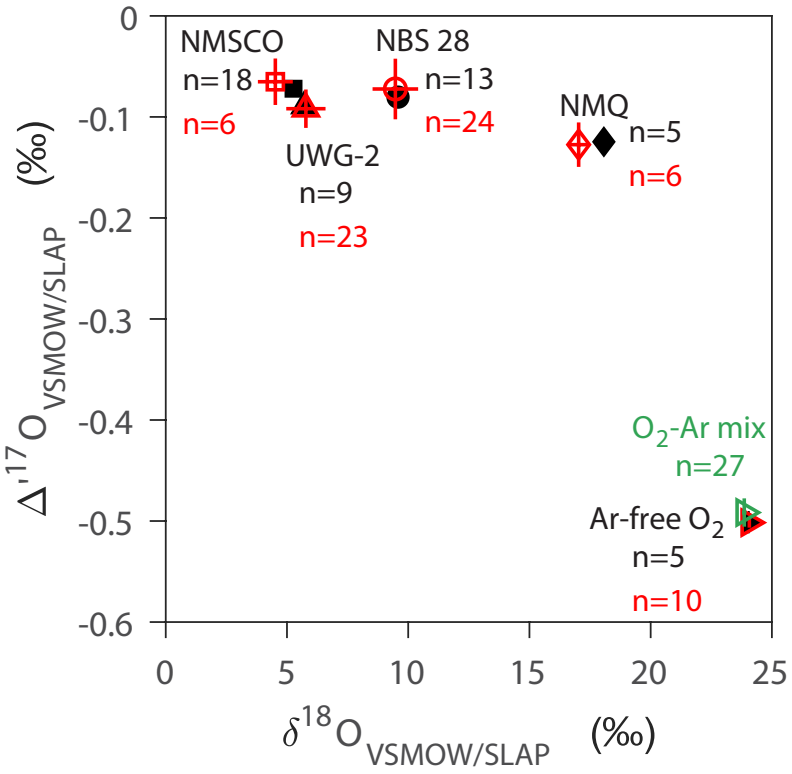

Fig. S1. A comparison of four silicate standards and atmopsheric O_2 measurements between the Johnston lab (red markers and green marker) and recently published values (1) (black markers). Error bars reflect 1σ uncertainty. The number of measurements for each standard is reflected by 'n'.

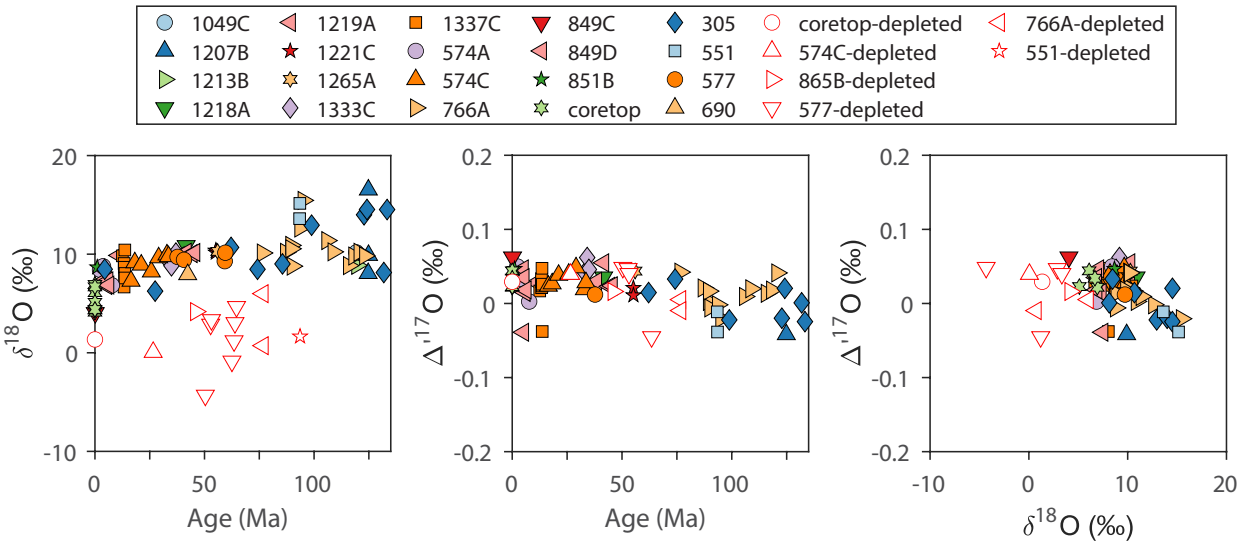

Fig. S2. The full dataset of barite δ^{18}O (left panel, y-axis) and Δ'^{17}O (middle panel, y-axis) is plotted above, over the last 130 million years (left and middle panels, x-axes). In the right panel, Δ'^{17}O (y-axis) is plotted against δ^{18}O (x-axis). Samples are denoted by filled circles or triangles, with associated error bars (0.3‰ for δ^{18}O and 0.020‰ for Δ'^{17}O). Samples from Site 577 are denoted by filled orange circles. In all panels, low δ^{18}O outliers from the global record are denoted by white-filled markers with a red outline.

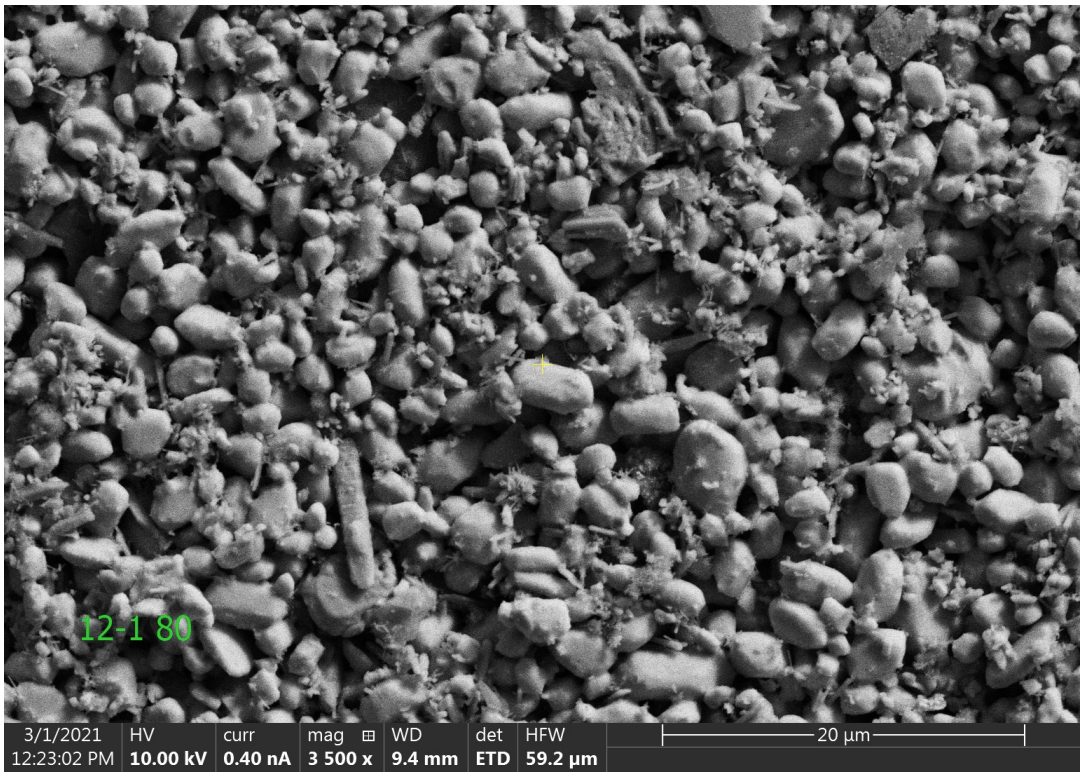

Fig. S3. An SEM image of extracted barite (pre-Na_2CO_3 processing) from site 577 (577 12-1 80-86cm) is pictured above. The well-defined crystals are barites and the amorphous solids are indicative of contaminating phases. This sample has an abundance of non-barite phases and was identified as an outlier based on $\delta^{18}O$.

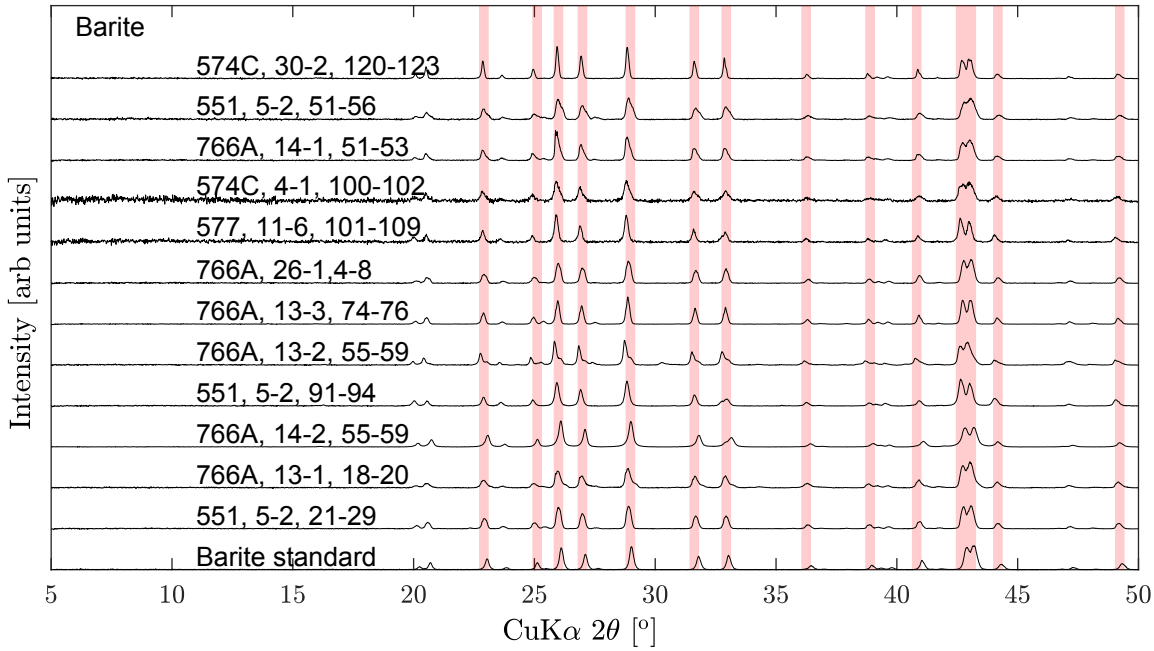

Fig. S4. XRD patterns for a subset of Na_2CO_3-reprocessed samples.

We finally note that samples that are offset in $\delta^{18}O$ do not deviate significantly from the $\Delta'^{17}O$ trends (Figure S2, center panel). The lack of anomalous $\Delta'^{17}O$ is, in some sense, to be expected. If the mechanism underlying the alteration of the pristine barite is mass-dependent, we would expect a complementary deviation in $\Delta'^{17}O$ at or within our statistical uncertainty. For instance, a 5‰ offset in $\delta^{18}O$ generated by a process that carries a typical mass-dependent θ value (0.525 in this example) would only produce a 0.025‰ effect in $\Delta'^{17}O$, which is at the edge of our 1σ confidence interval. Given that the $\Delta'^{17}O$ of the $\delta^{18}O$ outliers falls in the same range as the rest of the time series data, their inclusion or exclusion does not change the result or interpretation.

Determining marine sulfate isotopic composition. A constant correction factor, calibrated in previous work (7), is applied to the entire barite dataset in order to determine the record of seawater sulfate isotopic composition. Comparison of coretop (youngest, most recently sedimented) marine barite measurements to modern seawater sulfate have shown that the barite mineral is depleted in $\delta^{18}O$ by 3.0±0.8‰, relative to dissolved sulfate, while there is no significant offset in $\Delta'^{17}O$ (7, 8, 15, 16). Furthermore, the small isotopic fractionation associated with marine sulfate precipitation should have remained constant through time. Here we determine seawater sulfate composition by applying a correction factor of -3.0‰ to the full barite $\delta^{18}O$ record, and a confidence interval of 3σ=2.4‰. No treatment is applied to the $\Delta'^{17}O$ record, and these values are interpreted to directly reflect contemporaneous seawater sulfate composition.

Testing the covariance in marine sulfate $\delta^{18}O$ and $\delta^{34}S$. We determined the covariance of the smoothed records of marine sulfate $\delta^{18}O$ and $\delta^{34}S$ across 5 million year intervals. Smoothed values were calculated for $\delta^{18}O$ and $\delta^{34}S$ at a time step of 0.1 million years. Then the smoothed values were binned into 5 million year intervals, and the covariance calculated. The resulting covariance was positive or close to zero for ages <40 million years (see Figure S5), meaning that $\delta^{18}O$ and $\delta^{34}S$ covary positively or do not covary. For the values >80 million years where there is less data density, the covariance is high and oscillates more.

Details of the two-component mixing model. The oxygen isotope composition (here just $\delta^{18}O$) of marine sulfate can be effectively interpreted as a system at steady state due to its short residence time relative to the rate of isotopic change. We apply the two-component mixing model framework developed for the modern seawater sulfate reservoir (16) to the time series record. The mixing equation is cast as:

$$ {}^{1x}R_{seawater} = \frac{{}^{1x}R_{bio} \cdot J_{bio} + {}^{1x}R_{riv} \cdot J_{riv}}{J_{bio} + J_{riv}} \quad [1] $$

where R is an isotope composition. Constraining the isotopic composition of each endmember allows for a prediction of the relative size of each flux (J_{bio}/J_{riv}). In Figure S6, the $\delta^{18}O$ record of marine sulfate is used to calculate the relative flux sizes J_{bio}/J_{riv} (left y-axis, black line).

While we cannot disentangle the possible time-dependence of the endmember isotope compositions from their relative sizes, we perform a test for each case. First, we hold the endmember sulfate isotope compositions constant and determine the resulting J_{bio}/J_{riv} ratio that best describes the marine sulfate record (Figure S6, left y-axis). Second, we hold the ratio J_{bio}/J_{riv} constant and determine the resulting isotopic composition of riverine sulfate input that satisfies the marine sulfate record (Figure S6, right y-axis). The resulting shape of each curve is identical. The higher degree of variation reflected in the Cretaceous (>65 Ma) than the Cenozoic (modern to 65 Ma) is likely correlated with the projected lower $[SO_4^{2-}]$ (5 to 14mM) during this time interval than today (28mM) (17, 20–22). Since the model assumes steady-state, it does not capture the modulating effect of a potential increased residence time on marine sulfate isotope composition. Therefore we focus our interpretation on the relative differences in modeled flux sizes and isotope compositions across long timescales.

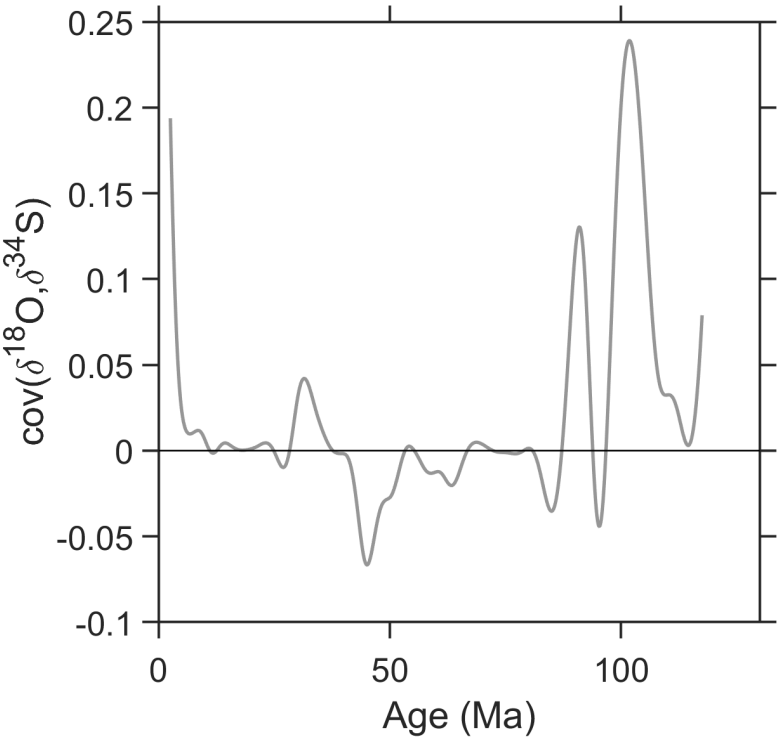

Fig. S5. Calculated covariance between seawater sulfate δ^{18}O and δ^{34}S (y-axis) versus time in millions of years (x-axis). The black horizontal line at covariance=0 is included for reference.

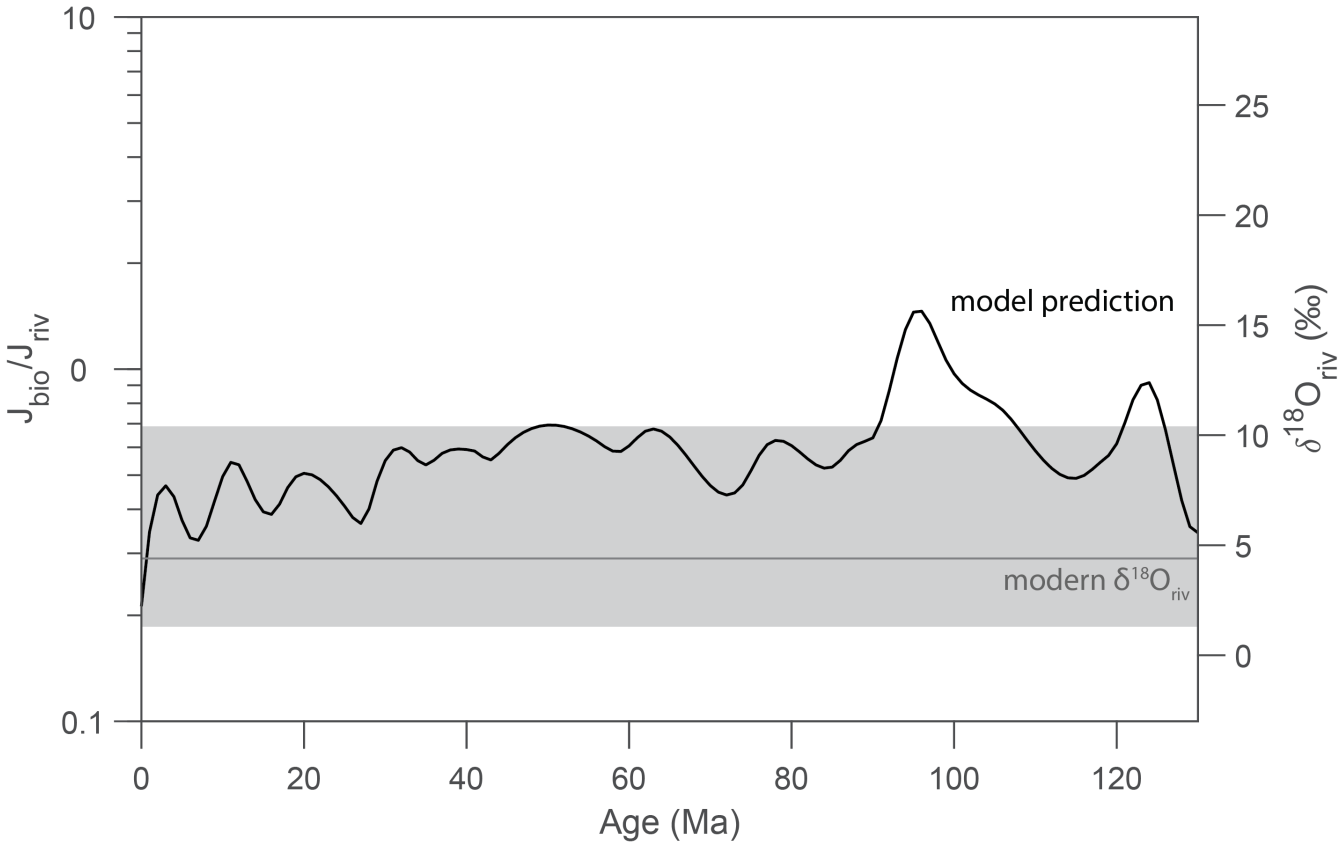

Fig. S6. Results from the two-flux model are plotted as a solid black line, which reflects either J_{bio}/J_{riv} (left y-axis) or $\delta^{18}O_{riv}$ (right y-axis). The ratio J_{bio}/J_{riv} is calculated with inputs $\delta^{18}O_{riv}$=4.4‰ and $\delta^{18}O_{bio}$=27.3‰. The resulting $\delta^{18}O_{riv}$ is determined by constraining J_{riv}/J_{bio}=4.8 and $\delta^{18}O_{bio}$=27.3‰. The interquartile range of $\delta^{18}O$ from modern rivers is represented by the gray shaded region, with the modern river $\delta^{18}O$ mean as a solid gray line at 4.4‰ (Dataset S4).

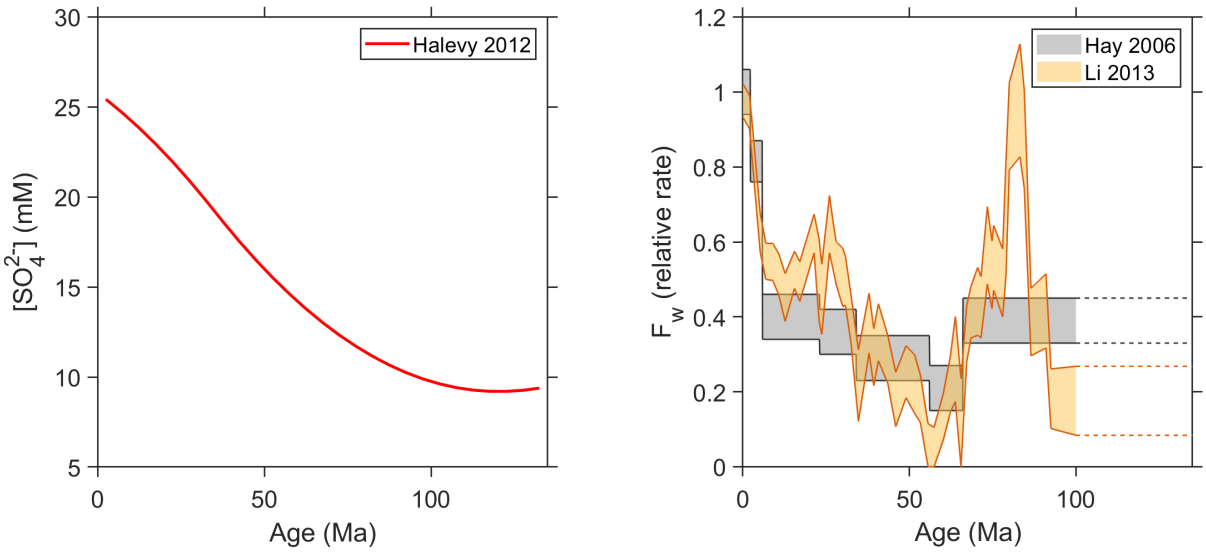

Fig. S7. Time series inputs of $[SO_4^{2-}]$ (based on fluid inclusion data (17)) and predicted weathering fluxes J_{riv} (based on the sedimentary rock record (18) and a global carbon cycle model (19)), to the sulfur cycle model are shown above.

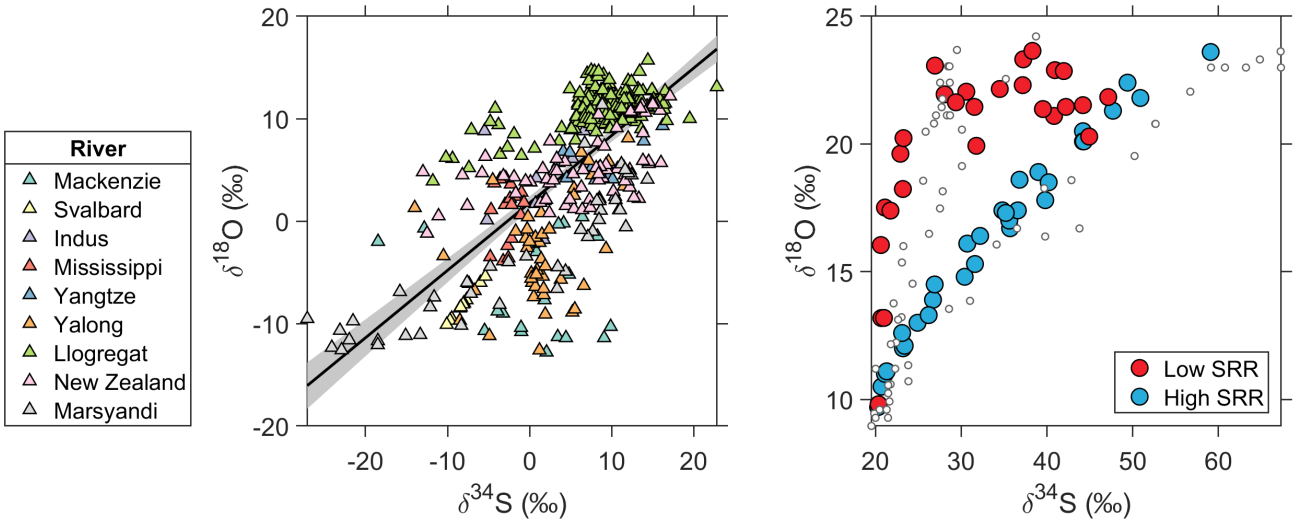

Fig. S8. Compilations of sulfate stable isotope measurements (δ^{18}O and δ^{34}S) for modern rivers (panel a, (23)) and for modern pore waters with varying rates of sulfate reduction (panel b, (8)) are plotted above.

SI Dataset S1 (dataset_one.xlsx)
Full marine barite sample information with GTS 2012 age model and corrected $\delta^{18}O$ and $\Delta'^{17}O$.

SI Dataset S2 (dataset_two.xlsx)
Global compilation of river sulfate isotope measurements (n=919).

References

1. Wostbrock JA, Cano EJ, Sharp ZD (2020) An internally consistent triple oxygen isotope calibration of standards for silicates, carbonates and air relative to VSMOW2 and SLAP2. *Chemical Geology* 533:119432.
2. Paytan A, Kastner M, Campbell D, Thiemens MH (1998) Sulfur isotopic composition of Cenozoic seawater sulfate. *Science* 282(5393):1459–1462.
3. Paytan A, Kastner M, Chavez F (1996) Glacial to interglacial fluctuations in productivity in the equatorial Pacific as indicated by marine barite. *Science* 274(5291):1355–1357.
4. Paytan A, Kastner M, Martin E, Macdougall J, Herbert T (1993) Marine barite as a monitor of seawater strontium isotope composition. *Nature* 366(6454):445–449.
5. Von Allmen K, Böttcher ME, Samankassou E, Nägler TF (2010) Barium isotope fractionation in the global barium cycle: First evidence from barium minerals and precipitation experiments. *Chemical Geology* 277(1-2):70–77.
6. Breit GN, Simmons E, Goldhaber M (1985) Dissolution of barite for the analysis of strontium isotopes and other chemical and isotopic variations using aqueous sodium carbonate. *Chemical Geology: Isotope Geoscience section* 52(3-4):333–336.
7. Markovic S, Paytan A, Li H, Wortmann UG (2016) A revised seawater sulfate oxygen isotope record for the last 4 Myr. *Geochimica et Cosmochimica Acta* 175:239–251.
8. Johnston DT, et al. (2014) Placing an upper limit on cryptic marine sulphur cycling. *Nature* 513(7519):530–533.
9. Eagle M, Paytan A, Arrigo KR, van Dijken G, Murray RW (2003) A comparison between excess barium and barite as indicators of carbon export. *Paleoceanography* 18(1).
10. Paytan A, Mearon S, Cobb K, Kastner M (2002) Origin of marine barite deposits: Sr and S isotope characterization. *Geology* 30(8):747–750.
11. Yao W, et al. (2020) A revised seawater sulfate S-isotope curve for the eocene. *Chemical Geology* 532:119382.
12. Paytan A, Kastner M, Campbell D, Thiemens MH (2004) Seawater sulfur isotope fluctuations in the Cretaceous. *Science* 304(5677):1663–1665.
13. DeBond N, Oakes RL, Paytan A, Wortmann UG (2012) Early aptian carbon and sulphur isotope signatures at ODP Site 765. *Isotopes in environmental and health studies* 48(1):180–194.
14. Marenco PJ, Corsetti FA, Hammond DE, Kaufman AJ, Bottjer DJ (2008) Oxidation of pyrite during extraction of carbonate associated sulfate. *Chemical Geology* 247(1-2):124–132.
15. Waldeck AR, et al. (2022) Calibrating the triple oxygen isotope composition of evaporite minerals as a proxy for marine sulfate. *Earth and Planetary Science Letters* 578:117320.
16. Waldeck A, et al. (2019) Deciphering the atmospheric signal in marine sulfate oxygen isotope composition. *Earth and Planetary Science Letters* 522:12–19.
17. Halevy I, Peters SE, Fischer WW (2012) Sulfate burial constraints on the phanerozoic sulfur cycle. *Science* 337(6092):331–334.
18. Hayes JM, Waldbauer JR (2006) The carbon cycle and associated redox processes through time. *Philosophical Transactions of the Royal Society B: Biological Sciences* 361(1470):931–950.
19. Li G, Elderfield H (2013) Evolution of carbon cycle over the past 100 million years. *Geochimica et Cosmochimica Acta* 103:11–25.
20. Timofeeff MN, Lowenstein TK, Da Silva MAM, Harris NB (2006) Secular variation in the major-ion chemistry of seawater: Evidence from fluid inclusions in cretaceous halites. *Geochimica et Cosmochimica Acta* 70(8):1977–1994.
21. Lowenstein TK, Hardie LA, Timofeeff MN, Demicco RV (2003) Secular variation in seawater chemistry and the origin of calcium chloride basinal brines. *Geology* 31(10):857–860.
22. Horita J, Zimmermann H, Holland HD (2002) Chemical evolution of seawater during the phanerozoic: Implications from the record of marine evaporites. *Geochimica et Cosmochimica Acta* 66(21):3733–3756.
23. Hemingway JD, et al. (2020) Triple oxygen isotope insight into terrestrial pyrite oxidation. *Proceedings of the National Academy of Sciences* 117(14):7650–7657.